Hindawi Publishing Corporation
EURASIP Journal on Advances in Signal Processing
Volume 2007, Article ID 38916, 10 pages
doi:10.1155/2007/38916

Research Article

Wavelet-Based Algorithm for Signal Analysis

Norman C. F. Tse[1] and L. L. Lai[2]

[1] *Division of Building Science and Technology, City University of Hong Kong, Tat Chee Avenue, Kowloon, Hong Kong*
[2] *School of Engineering and Mathematical Sciences, City University, Northampton Square, London EC1V0HB, UK*

Received 6 August 2006; Revised 12 October 2006; Accepted 24 November 2006

Recommended by Irene Y. H. Gu

This paper presents a computational algorithm for identifying power frequency variations and integer harmonics by using wavelet-based transform. The continuous wavelet transform (CWT) using the complex Morlet wavelet (CMW) is adopted to detect the harmonics presented in a power signal. A frequency detection algorithm is developed from the wavelet scalogram and ridges. A necessary condition is established to discriminate adjacent frequencies. The instantaneous frequency identification approach is applied to determine the frequencies components. An algorithm based on the discrete stationary wavelet transform (DSWT) is adopted to denoise the wavelet ridges. Experimental work has been used to demonstrate the superiority of this approach as compared to the more conventional one such as the fast Fourier transform.

1. INTRODUCTION

Power quality has become a major concern for utility, facility, and consulting engineers in recent years. International as well as local standards have been formulated to address the power quality issues [1]. To the facility managers and end users, frequent complaints by tenants/customers on occasional power failures of computer and communication equipment and the energy inefficiency of the LV electrical distribution system are on the management's agenda. Harmonic currents produced by nonlinear loads would cause extra copper loss in the distribution network, which on one hand will increase the energy cost and on the other hand would increase the electricity tariff charge. The benefits of using power electronic devices in the LV distribution system in buildings, such as switch mode power supplies, variable speed drive units, to save energy are sometimes offset by the increased energy loss in the distribution cables by current harmonics and the cost of remedial measures required. Voltage harmonics caused by harmonic voltage drops in the distribution cables are affecting the normal operation of voltage-sensitive equipment as well.

In order to improve electric power quality and energy efficiency, the sources and causes of such disturbance must be known on demand sides before appropriate corrective or mitigating actions can be taken [2, 3].

A traditional approach is to use discrete Fourier transform (DFT) to analyze harmonics contents of a power signal. The DFT which is implemented by FFT has many attractive features. That theory of FFT has been fully developed and well known; scientists and engineers are familiar with the computation procedures and find it convenient to use as many standard computation tools as readily available. It is however easily forgotten that Fourier transform is basically a steady-state analysis approach. Transient signal variations are regarded by FFT as a global phenomenon.

Nowadays power quality issues, such as subharmonics, integer harmonics, interharmonics, transients, voltage sag and swell, waveform distortion, power frequency variations, are experienced by electricity users. This paper attempts to develop an algorithm based on continuous wavelet transform to identify harmonics in a power signal [4].

2. WAVELET TRANSFORM AND ANALYZING WAVELET

Wavelet transform (WT) has been drawing many attentions from scientists and engineers over the years due to its ability to extract signal time and frequency information simultaneously. WT can be continuous or discrete. Continuous wavelet transform (CWT) is adopted for harmonic analysis because of its ability to preserve phase information [5, 6].

The wavelet transform of a continuous signal, $f(t)$, is defined as [5],

$$Wf(u,s) = \langle f, \psi_{u,s} \rangle = \int_{-\infty}^{+\infty} f(t) \frac{1}{\sqrt{s}} \Psi^* \left(\frac{t-u}{s} \right) dt, \quad (1)$$

where $\psi^*(t)$ is the complex conjugate of the wavelet function $\psi(t)$; s is the dilation parameter (scale) of the wavelet; and u is the translation parameter (location) of the wavelet.

The wavelet function must satisfy certain mathematical criteria [7]. These are the following:

(i) a wavelet function must have finite energy; and
(ii) a wavelet function must have a zero mean, that is, has no zero frequency component.

The simplified complex Morlet wavelet (CMW) [8, 9] is adopted in the algorithm for harmonic analysis as shown in Figure 1, defined as

$$\Psi(t) = \frac{1}{\sqrt{\pi f_b}} e^{-t^2/f_b} e^{j2\pi f_c t}, \quad (2)$$

where f_b is the bandwidth parameter and f_c is the center frequency of the wavelet.

The CMW is essentially a modulated Gaussian function. It is particularly useful for harmonic analysis due to its smoothness and harmonic-like waveform. Because of the analytic nature, CMW is able to separate amplitude and phase information.

Strictly speaking, the mean of the simplified CMW in (2) is not equal to zero as illustrated in (3),

$$\int_{-\infty}^{+\infty} \Psi(t) dt = \frac{1}{\sqrt{\pi f_b}} \int_{-\infty}^{+\infty} e^{j2\pi f_c t} e^{-t^2/f_b} dt = e^{(-f_b/4)(2\pi f_c)^2}. \quad (3)$$

However the mean of the CMW can be made arbitrarily small by picking the f_b and f_c parameters large enough [9]. For example, the mean of the CMW in (3) with $f_b = 2$ and $f_c = 1$ is 2.6753×10^{-9} which is practically equal to zero. The frequency support of the CMW in (2) is not a compact support but the entire frequency axis. The effective time support of the CMW in (2) is from -8 to 8 [10] provided that f_b is not larger than 9.

From the classical uncertainty principle, it is well known that there is a fundamental trade-off between the time and frequency localization of a signal. In other words, localization in one domain necessarily comes at the cost of localization in the other. The time-frequency localization is measured in the mean squares sense and is represented as a Heisenberg box. The area of the Heisenberg box is limited by

$$\delta\omega \delta t \geq \frac{1}{2}, \quad (4)$$

where $\delta\omega$ is the frequency resolution, and δt is the time resolution.

For a dilated complex Morlet wavelet,

$$\delta\omega = \frac{1}{s\sqrt{f_b}}, \qquad \delta t = \frac{s\sqrt{f_b}}{2}. \quad (5)$$

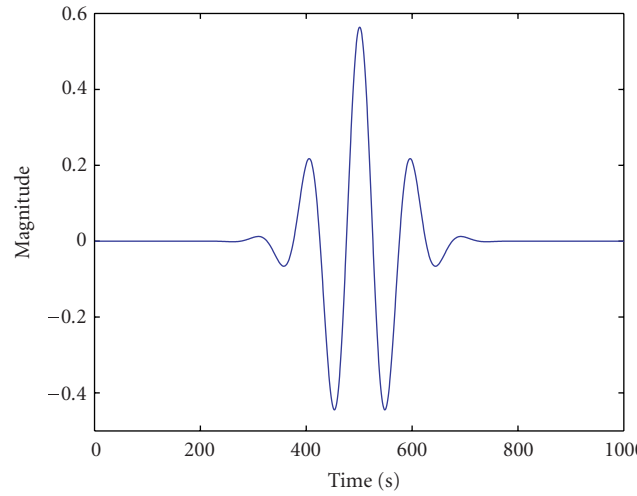

(a) Real part

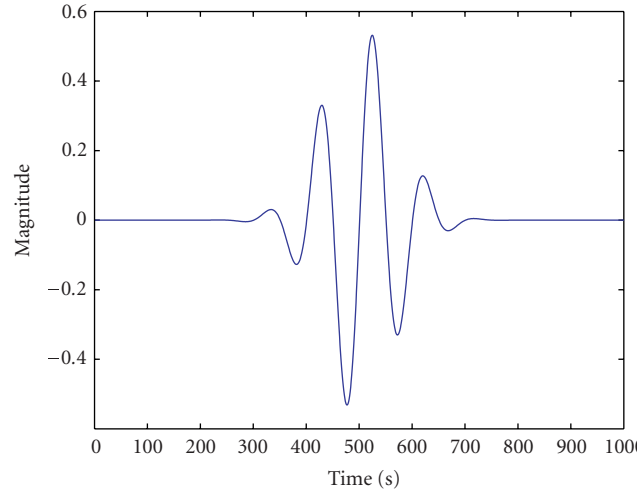

(b) Imaginary part

Figure 1: The real part and imaginary part of the complex Morlet wavelet.

Complex Morlet Wavelet achieves a desirable compromise between time resolution and frequency resolution, with the area of the Heisenberg box equal to 0.5. From (5), it is seen that the frequency resolution is dependent on the selection of f_b and the dilation. As will be discussed in Section 4, the dilation is dependent on the selection of f_c and the sampling frequency.

3. HARMONICS FREQUENCY DETECTION

Given a signal $f(t)$ represented as

$$f(t) = a(t) \cos \phi(t), \quad (6)$$

the wavelet function in (2) can be represented as [11],

$$\Psi(t) = g(t) e^{j\omega t}. \quad (7)$$

The dilated and translated wavelet families [11] are represented as

$$\Psi_{u,s}(t) = \frac{1}{\sqrt{s}}\Psi\left(\frac{t-u}{s}\right) = e^{-j\xi u}g_{s,u,\xi}(t), \tag{8}$$

where $g_{s,u,\xi}(t) = \sqrt{s}g((t-u)/s)e^{j\xi t}$; and $\xi = \omega/s$.

The wavelet transform of the signal function $f(t)$ in (6) is given as [11],

$$Wf(u,s) = \frac{\sqrt{s}}{2}a(u)e^{j\phi(u)}(\hat{g}(s[\xi - \phi'(u)]) + \varepsilon(u,\xi)), \tag{9}$$

where $\hat{g}(\omega)$ represents the Fourier transform of the function $g(t)$.

The corrective term $\varepsilon(u,\xi)$ in (9) is negligible if $a(t)$ and $\phi'(t)$ in (6) have small variations over the support of $\psi_{u,s}$ in (8) and if $\phi'(u) \geq \Delta\omega/s$ [11]. If a power signal contains only a single frequency, the corrective term can be neglected safely. However for a power signal containing harmonics from low frequency to high frequency, the corrective term will contribute to the wavelet coefficients, making the frequency detection not straightforward.

The instantaneous frequency is measured from wavelet ridges defined over the wavelet transform. The normalised scalogram defined by [11, 12]

$$\frac{\xi}{\eta}P_w f(u,\xi) = \frac{|Wf(u,s)|^2}{s} \tag{10}$$

is calculated with

$$\frac{\xi}{\eta}P_w f(u,\xi) = \frac{1}{4}a^2(u)\left|\hat{g}\left(\eta\left[1 - \frac{\phi'(u)}{\xi}\right]\right) + \varepsilon(u,\xi)\right|^2. \tag{11}$$

Since $|\hat{g}(\omega)|$ in (11) is maximum at $\omega = 0$, if one neglects $\varepsilon(u,\xi)$, (11) shows that the scalogram is maximum at

$$\frac{\eta}{s(u)} = \xi(u) = \phi'(u). \tag{12}$$

The corresponding points $(u, \xi(u))$ calculated by (12) are called wavelet ridges [13]. For the complex Morlet wavelet, $g(t)$ in (7) is a Gaussian function. Since the Fourier transform of a Gaussian function is also a Gaussian function, the wavelet ridge plot exhibits a Gaussian shape.

Figure 2 shows the wavelet ridges plot for a 40 Hz signal. It can be seen that the wavelet ridges can accurately detect the frequency of the signal.

Figure 3 shows the wavelet ridges plot for the detection of a 40 Hz signal component in a signal containing frequencies at 40 Hz and 240 Hz, respectively. There are some fluctuations at the peak of the wavelet ridges, introducing small errors in the frequency detection. The fluctuations are due to imperfection of the filters produced by the dilated CMWs and the corrective term in (9).

Discrete stationary Wavelet transform (DSWT) [14] is adopted to remove the fluctuations of the wavelet ridges. In view of the shape of the wavelet ridges, the Symlet2 wavelet

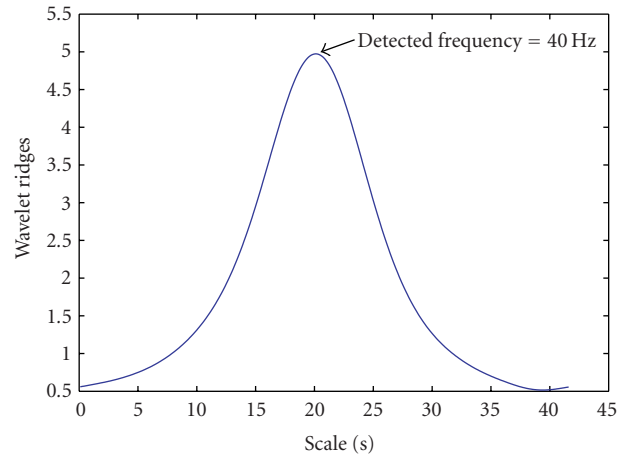

Figure 2: Wavelet ridges plot for a 40 Hz signal.

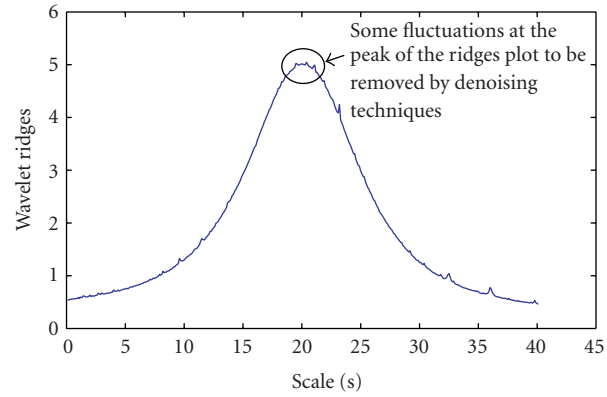

Figure 3: Wavelet ridges plot for a 40 Hz signal component in signal containing 40 Hz and 240 Hz.

developed by Daubechies is used. It is found that a decomposition level of 5 is sufficient to remove the fluctuations. Figure 4 shows the denoised wavelet ridges plot of the signal containing frequencies at 40 Hz and 240 Hz, respectively. The 40 Hz frequency component of the signal is accurately detected by the wavelet ridges after denoising.

4. DISCRIMINATION OF ADJACENT FREQUENCIES

The Fourier transform of a dilated CMW in (8) is represented as [11]

$$\Psi(sf) = \sqrt{s}e^{-\pi^2 f_b(sf-f_c)^2}. \tag{13}$$

The function $\Psi(sf)$ can be regarded as a bandpass filter centered at the frequency f_c. The bandwidth of the bandpass filter can be adjusted by adjusting f_b. The CWT of a signal is the convolution of the signal with a group of bandpass filters which is produced by the dilation of the CMW.

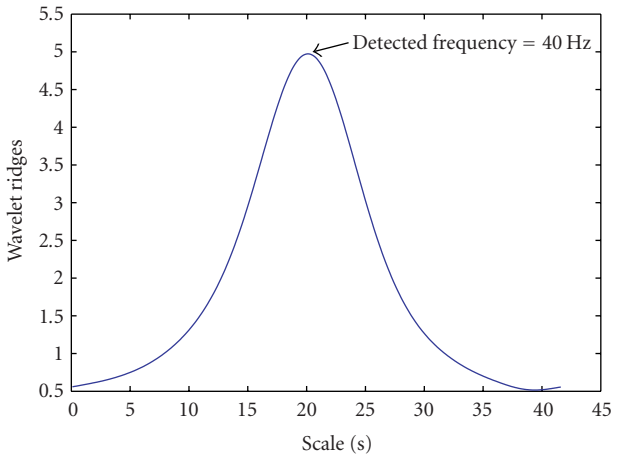

Figure 4: Denoised wavelet ridges plot of the wavelet ridges plot in Figure 3.

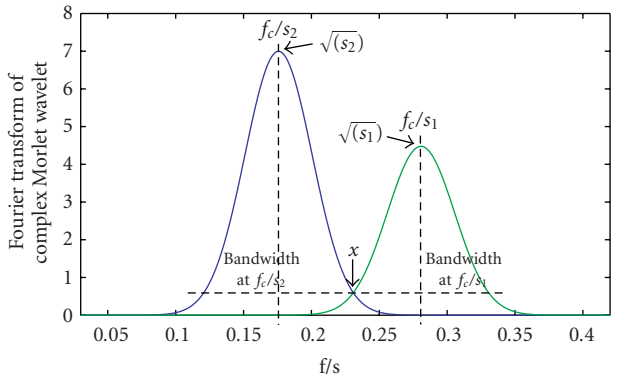

Figure 5: Frequency plot of (15) for two CMWs at scales S_1 and S_2, respectively.

Suppose that (13) is represented as

$$\Psi(sf) = x, \tag{14}$$

where x represents an arbitrary magnitude to be defined later.

Combining (13) and (14) gives

$$f = \frac{f_c}{s} \pm \frac{1}{s\pi\sqrt{f_b}}\sqrt{\left|\ln\left(\frac{x}{\sqrt{s}}\right)\right|}, \tag{15}$$

where f_c/s is the center frequency of the dilated bandpass filter; and the bandwidth is $(2/s\pi\sqrt{f_b})\sqrt{|\ln(x/\sqrt{s})|}$.

Figure 5 shows the plot of the frequency support of two dilated CMWs at scales S_1 and S_2, respectively.

If the two dilated CMWs are used to detect two adjacent frequencies in a signal, with their frequencies represented as [10]

$$f_1 = \frac{f_s f_c}{S_1}, \qquad f_2 = \frac{f_s f_c}{S_2}, \tag{16}$$

where f_s represents the sampling frequency, then

$$\frac{f_c}{S_1} - \frac{f_c}{S_2} = \frac{1}{S_1\pi\sqrt{f_b}}\sqrt{\left|\ln\left(\frac{x}{\sqrt{S_1}}\right)\right|} + \frac{1}{S_2\pi\sqrt{f_b}}\sqrt{\left|\ln\left(\frac{x}{\sqrt{S_2}}\right)\right|}. \tag{17}$$

Assume that $S_2 > S_1$, (17) is simplified to

$$f_c\sqrt{f_b} > \frac{1}{\pi}\sqrt{\left|\ln\left(\frac{x}{\sqrt{S_1}}\right)\right|}\, x\frac{f_2 + f_1}{f_2 - f_1}. \tag{18}$$

For $S_1 = 200$ and $x = 0.5$,

$$\frac{1}{\pi}\sqrt{\left|\ln\left(\frac{x}{\sqrt{S_1}}\right)\right|} = 0.58. \tag{19}$$

Substituting (19) into (18) gives

$$f_c\sqrt{f_b} > 0.58\, x\frac{f_2 + f_1}{f_2 - f_1}, \quad S_1 \le 200, \quad x \le 0.5. \tag{20}$$

It is estimated that the magnitude of x should not be larger than 0.5. Equation (20) is used to determine the values of f_b and f_c in (2) for the continuous wavelet transform with complex Morlet wavelet which is a necessary condition to discriminate adjacent frequencies contained in the power signal.

5. HARMONICS AMPLITUDE DETECTION

Theoretically, once the algorithms developed in Sections 3 and 4 detect the harmonics contained in the power signal, the corresponding harmonics amplitudes would be determined readily by

$$\begin{aligned} a(u) &= \frac{2\sqrt{(\xi/\eta)P_w f(u,\xi)}}{|\hat{g}(0)|} = \frac{2\sqrt{|Wf(u,s)|^2/s}}{1} \\ &= \frac{2|Wf(u,s)|}{\sqrt{s}}. \end{aligned} \tag{21}$$

The values of $2\sqrt{|Wf(u,s)|^2/s}$ in (21) are produced in the process of generating the scalogram.

Due to the imperfection of the filters produced by the dilated CMWs and the corrective terms in (9), the amplitudes detected exhibit fluctuations. Simulation results show that the amplitudes for harmonics frequencies from 50 Hz to 1000 Hz have errors of the order of ±5%. Figure 6 shows a plot of the absolute wavelet coefficients generated by (21) for a 991.5 Hz harmonic frequency component of a power signal containing frequencies ranging from 50 Hz to 1000 Hz. The smoothness of the absolute wavelet coefficients plot is also related to the number of data points taken per cycle of the harmonic frequency component. It is found that a minimum of 25 data points per cycle should be used to provide a smoother absolute wavelet coefficients plot.

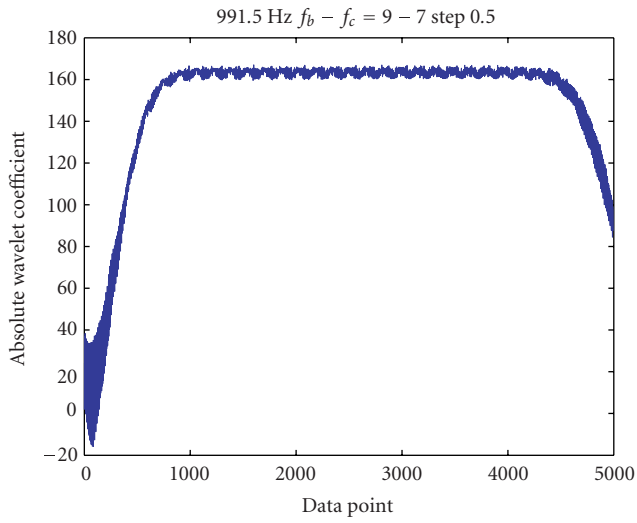

Figure 6: Absolute wavelet coefficients plot generated by CWT (using complex Morlet wavelet, $f_b = 9$, $f_c = 7$) for harmonic frequency at 991.5 Hz.

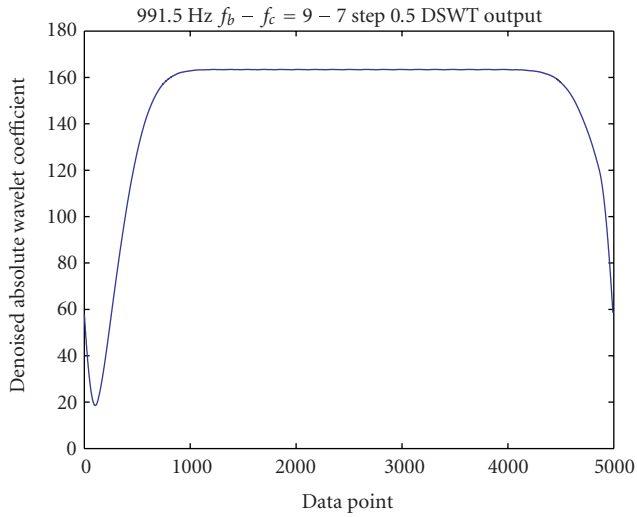

Figure 7: Coefficients generated by discrete stationary wavelet transform (Haar wavelet, level 5 decomposition) of the absolute wavelet coefficients plot in Figure 6.

Discrete stationary wavelet transform (DSWT) [14] is adopted to remove the fluctuations. Since the absolute wavelet coefficients plot should exhibit a constant magnitude for a harmonic frequency of constant amplitudes, the Haar wavelet is used for the DSWT to denoise the absolute wavelet coefficients. It is found that a decomposition level of 5 is sufficient for harmonics up to 1000 Hz.

Figure 7 shows the output of the DSWT of the absolute wavelet coefficients shown in Figure 6. The fluctuations are removed resulting in an accurate detection of the amplitude of the harmonics frequency.

Table 1: Harmonics in the simulated signal.

Harmonics (Hz)	Amplitude	Phase angle (degree)
49.2	311	0
102	280	5
149.5	248	7
249	217	10
362	186	15
442	155	20
540	155	25
640	124	−30
770	93	42
902	62	−20

Table 2: Settings of the proposed detection algorithm.

Frequency range (Hz)	Sampling frequency (Hz)	Data length/time period (seconds)	f_b-f_c
40–75	5000	3000/0.6 s	6-2
75–275	7500	3000/0.4 s	6-2
275–575	15 000	3000/0.2 s	6-3
575–925	25 000	4000/0.16 s	6-3

6. THE PROPOSED HARMONICS DETECTION ALGORITHM

The proposed harmonics detection algorithm is presented in Figure 8.

The proposed algorithm is implemented with Matlab software.

7. SIMULATION SETTINGS

A simulated signal is used to test the proposed harmonics detection algorithm. The simulated signal contains signal frequency components as shown in Table 1. The simulated signal does not contain 50 Hz frequency component.

The simulated signal is sampled at 25 kHz. The number of data points per cycle of the highest harmonics of 890 Hz in the simulated signal is approximately 28. In any case, a minimum of 25 data points per cycle of any harmonics should be maintained for accurate amplitude detection. A higher sampling frequency would give a better detection of the amplitudes of the harmonics frequencies, but more data points are required resulting in slow computation. For faster CWT computation, the simulated signal will be down-sampled for the detection of lower harmonics. The down-sampling settings are as shown in Table 2. In accordance with the classical uncertainty principle, a larger time window is required at low frequencies, and a smaller time window is sufficient at high frequencies.

The necessary condition discussed in Section 4 for discrimination of adjacent frequencies requires that the complex Morlet wavelet should be set at $f_b = 6$ and $f_c = 2$ to 3 depending on the frequencies to be detected.

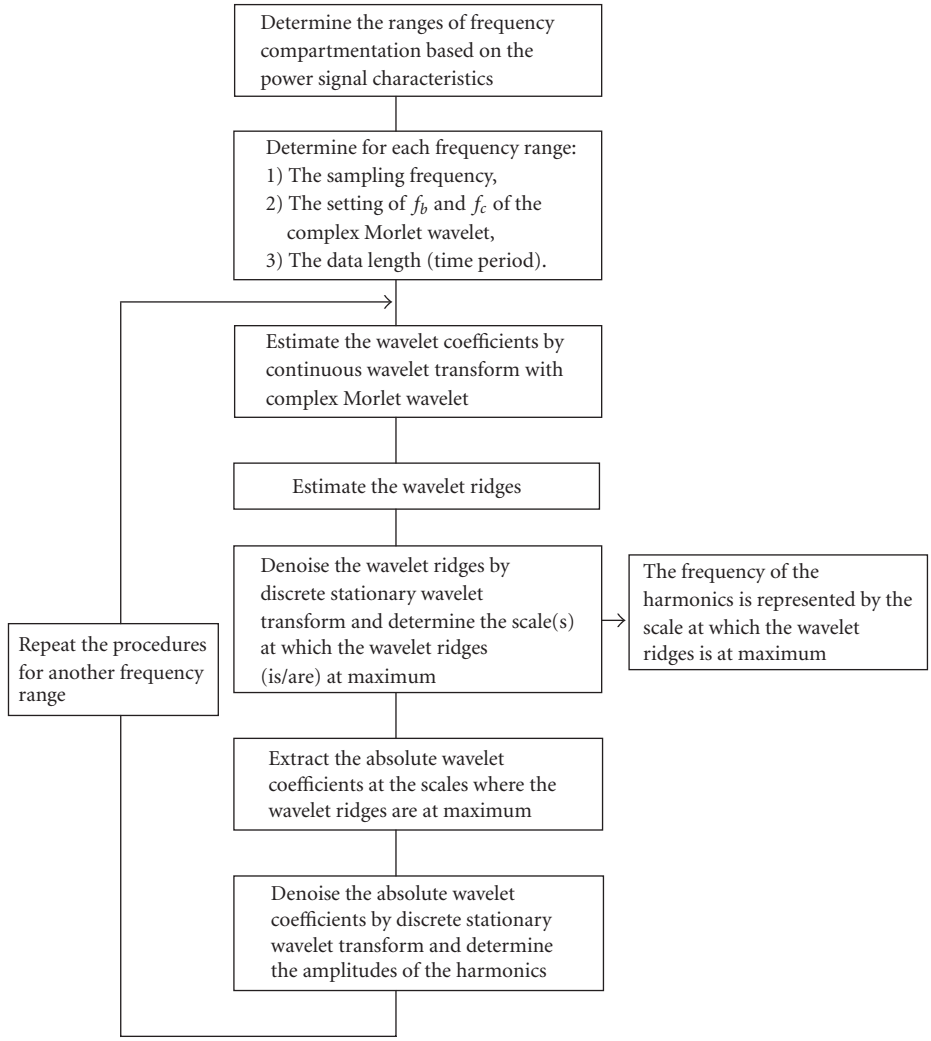

Figure 8: The flow chart of the proposed harmonics detection algorithm.

From (5) and (16), the frequency resolution is dependent on the bandwidth parameter f_b and the center frequency f_c of the dilated complex Morlet wavelet, and the sampling frequency f_s. For detection of higher harmonics, frequency resolution would be improved by using higher sampling frequency and larger f_b and f_c as shown in Table 2.

8. SIMULATION RESULTS

The simulation results for harmonics detection are shown in Table 3. It can be seen that the accuracy of the proposed algorithm is very promising. The small errors in the frequency detection are mainly due to the computation errors of the conversion from frequency to scale and vice versa. The scale increment size in the dilation of the wavelet, that is, the step size of the scales used in decomposition, is deterministic in the frequency detection accuracy. Higher resolution can be used if needed with a sacrifice in computation speed. It is proved that the necessary condition established in Section 4 is sufficient in distinguishing adjacent frequencies.

Table 3: Harmonics detection results.

Harmonics (Hz)	Detected harmonics (Hz)	% Error
49.2	49.19	0.02%
102	102.04	0.04%
149.5	149.55	0.03%
249	248.76	0.09%
362	362.1	0.03%
442	442.15	0.03%
540	539.57	0.08%
640	640.04	0.01%
770	770.18	0.02%
902	902.53	0.06%

The detection results of the amplitudes of the harmonics are very satisfactory, as shown in Table 4.

Table 4: Amplitudes detection results.

Harmonics (Hz)	Harmonics amplitude	Detected amplitude	% Error
49.2	311	311.05	0.02%
102	280	280.09	0.03%
149.5	248	248.12	0.05%
249	217	216.67	0.15%
362	186	185.98	0.01%
442	155	155.02	0.01%
540	155	154.63	0.22%
640	124	124.27	0.21%
770	93	92.99	0.01%
902	62	61.94	0.09%

Table 5 shows the FFT of the simulated signal for comparison. The sampling frequencies are set at 2 kHz and 25 kHz, respectively. A hamming window was applied to the data.

Table 6 shows the comparison of the detection errors of the proposed harmonic detection algorithm and the FFT. It can be seen that FFT has very good frequency detection capability, except for harmonic frequencies with decimal place. In the simulation test by FFT, the frequency detection errors are quite significant at harmonics of 49.2 Hz and 149.5 Hz. On amplitude detection, the proposed harmonics detection algorithm is more accurate than FFT for harmonic frequencies with decimal place.

9. EXPERIMENTAL RESULTS

Figure 9(a) shows a waveform captured from the red phase input current of a 3-phase 6-pulse variable speed drive (VSD) with the VSD output voltage set at 20 Hz. The sampling frequency is 10 kHz. The rated frequency of the low voltage electrical power supply source to the VSD is 50 Hz.

Figure 9(b) shows two cycles of the waveform in Figure 9(a). The shape of the waveform is a typical input current waveform of a 3-phase 6-pulse VSD. It is expected that the current would contain integer harmonics at 5th, 7th, 11th, 13th, 17th, 19th, and so forth harmonics of the fundamental frequency. Since the waveform is not exactly symmetrical, there are some even harmonics present in the waveform.

The proposed harmonics detection algorithm is used to analyze the waveform in Figure 9(a). Table 7 shows the ranges of frequency compartmentation, f_b and f_c settings of the complex Morlet wavelet, the sampling frequencies, data lengths, and time period used.

Table 8 shows the detection results, together with the results produced by FFT for comparison.

From Table 8, the fundamental frequency estimated by the proposed harmonics detection algorithm is 49.95 Hz. While FFT estimates that the fundamental frequency is 50 Hz , Table 9 compares the estimated harmonics by FFT and the proposed harmonics detection algorithm, respectively, to the integer multiples of respective fundamental frequencies.

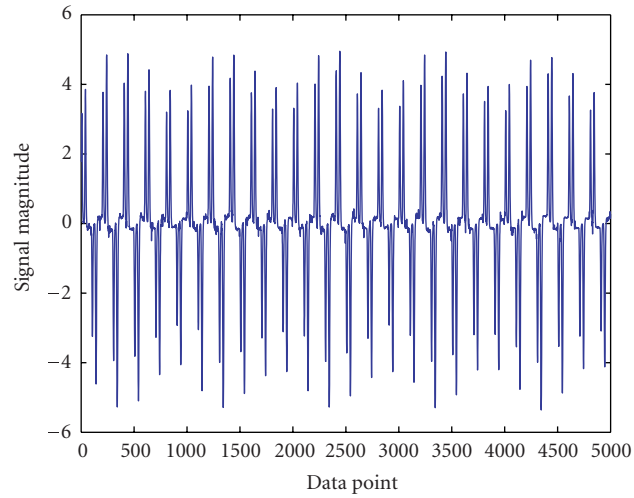

(a) Waveform of the red phase input current of a 3-phase 6-pulse variable speed drive (sampling frequency = 10 kHz).

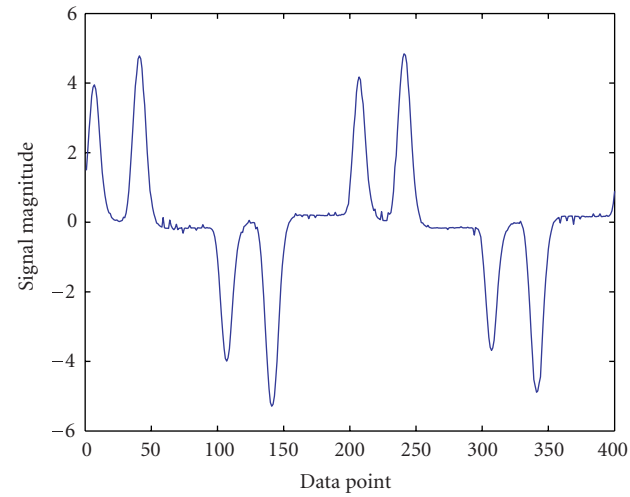

(b) Two cycles of the waveform in Figure 9(a).

Figure 9

For the proposed harmonics detection algorithm, the harmonics estimated conform to the integer multiples of the fundamental frequency at 49.95 Hz. Some deviations from the integer multiples of the fundamental frequency are however found only at even harmonics which have very small magnitudes.

The harmonics estimated by FFT do not conform to the integer multiples of the fundamental frequency estimated at 50 Hz. The errors are possibly due to the comparatively fine frequency resolution of 0.05 Hz. As a result, there are some frequency leakages in the FFT decomposition. The amplitudes of the harmonics estimated by FFT are therefore smaller than the amplitudes estimated by the proposed harmonic detection algorithm.

By counting zero crossings of the measured waveform, it was found that the average frequency for 50 cycles (time period = 1 s) of the fundamental frequency component is

Table 5: FFT of the simulated signal.

Harmonics (Hz)	Amp.	Sampling rate = 2 kHz Data length = 2000 Time period = 1 s		Sampling rate = 25 kHz Data length = 25000 Time period = 1 s	
		Detected freq. (Hz)	Detected amp.	Detected freq. (Hz)	Detected amp.
49.2	311	49	301.2	49	301.3
102	280	102	279.8	102	279.9
149.5	248	150	202.8	150	202.8
249	217	249	216.9	249	217
362	186	362	185.9	362	186
442	155	442	155	442	155
540	155	540	155	540	155
640	124	640	124	640	124
770	93	770	92.98	770	92.97
902	62	902	62.03	902	62.01

Table 6: Comparison of simulation results by the proposed detection algorithm and FFT.

Proposed detection algorithm		FFT			
		Sampling rate = 2 kHz Data length = 2000 Time period = 1 s		Sampling rate = 25 kHz Data length = 25000 Time period = 1 s	
Freq. error	Amp. error	Freq. error	Amp. error	Freq. error	Amp. error
0.02%	0.02%	0.41%	3.15%	0.41%	3.12%
0.04%	0.03%	0%	0.07%	0%	0.04%
0.03%	0.05%	0.33%	18.23%	0.33%	18.23%
0.09%	0.15%	0%	0.05%	0%	0%
0.03%	0.01%	0%	0.05%	0%	0%
0.03%	0.01%	0%	0%	0%	0%
0.08%	0.22%	0%	0%	0%	0%
0.01%	0.21%	0%	0%	0%	0%
0.02%	0.01%	0%	0.02%	0%	0.03%
0.06%	0.09%	0%	0.05%	0%	0.02%

Table 7: Settings of the proposed detection algorithm.

Frequency range (Hz)	f_b-f_c	Sampling frequency (Hz)	Data length/time period (seconds)
40–75	6-1	5000	5000/1 s
75–125	6-3	5000	5000/1 s
125–225	6-3	10 000	5000/0.5 s
225–375	6-3	10 000	5000/0.5 s
375–975	6-6	10 000	5000/0.5 s

49.95 Hz. This serves to confirm that the fundamental frequency estimated by the proposed harmonics detection algorithm is very accurate.

10. CONCLUSIONS

The proposed harmonics detection algorithm is able to identify the frequency and amplitude of harmonics in a power signal to a very high accuracy. The accuracy of the proposed harmonic detection algorithm has been verified by tests conducted to a computer-simulated signal and a field signal. Two techniques are adopted to achieve accurate frequency identification.

Firstly, complex Morlet wavelet is used for the continuous wavelet transform and secondly, wavelet ridges plot is used to extract the frequency information. Given that the complex Morlet wavelet is a Gaussian modulated function, the area of the Heisenberg box on the time-frequency plane is equal to 0.5. The bandwidth of the complex Morlet wavelet can be adjusted by carefully selecting the bandwidth

Table 8: Experimental results.

Harmonic no.	FFT with hamming window Sampling rate = 10 kHz Data length = 10000 Time period = 1 s		Proposed detection algorithm	
	Frequency	Amplitude	Frequency	Amplitude
1	50	1.521	49.95	1.547
2	100	0.06	99.93	0.069
3	150	0.284	149.85	0.303
4	200	0.051	199.6	0.066
5	250	1.209	249.79	1.351
7	350	0.861	349.65	1.014
8	400	0.029	398.94	0.038
9	450	0.117	449.78	0.137
10	500	0.016	500.83	0.024
11	550	0.451	549.45	0.564
12	Not detected	Not detected	597.61	0.015
13	649	0.256	649.35	0.307
15	749	0.04	748.13	0.048
17	849	0.118	848.66	0.131
19	949	0.043	949.37	0.054

Table 9: Comparison of accuracy in harmonics estimation.

Harmonic no.	FFT		Proposed detection algorithm	
	Expected frequency	Detected frequency	Expected frequency	Detected frequency
1	50	50	49.95	49.95
2	100	100	99.9	99.93
3	150	150	149.85	149.85
4	200	200	199.8	199.6
5	250	250	249.75	249.79
7	350	349.5	349.65	349.65
8	400	399.5	399.6	398.94
9	450	449.5	449.55	449.78
10	500	499.5	499.5	500.83
11	550	549.5	549.45	549.45
12	600	Not detected	599.4	597.61
13	650	649.5	649.35	649.35
15	750	749.5	749.25	748.13
17	850	849.5	849.15	848.66
19	950	949	949.05	949.37

parameter f_b and the dilation factor. The dilation factor in turn can be adjusted by the wavelet center frequency f_c and the sampling frequency. A narrow bandwidth is therefore achieved at the expense of time resolution. For an extremely narrow bandwidth, the time window would be large.

A second technique based on discrete stationary wavelet transform is adopted such that harmonic frequency can be determined accurately without the need of a large time window. It is seen that the wavelet ridges plot is a Gaussian; the scale at which the wavelet ridges plot is maximal represents the frequency of the harmonics in the signal. Discrete stationary wavelet transform is used to remove small fluctuations near the peak of the wavelet ridges plot so that a smooth Gaussian-like wavelet ridges plot is revealed, the peak of the wavelet ridges plot can then by identified.

Discrete stationary wavelet transform is proved to be useful in denoising the absolute wavelet coefficients of the continuous wavelet transform for amplitudes detection.

The disadvantage of the proposed algorithm is that the accuracy of both frequency and amplitude detections is dependent on the data points taken per cycle of the highest harmonics in the signal. In other words, a higher sampling frequency than twice the Nyquist frequency is required.

11. FURTHER WORKS

A future paper will show simulation results that the proposed harmonic detection algorithm could be used to detect noninteger harmonics. Further experimental tests would need to be conducted for noninteger harmonics detection as well as subharmonics detection.

REFERENCES

[1] "IEEE recommended practice for monitoring electric power quality," IEEE Standards Board, June 1995.

[2] L. L. Lai, W. L. Chan, C. T. Tse, and A. T. P. So, "Real-time frequency and harmonic evaluation using artificial neural networks," *IEEE Transactions on Power Delivery*, vol. 14, no. 1, pp. 52–59, 1999.

[3] W. L. Chan, A. T. P. So, and L. L. Lai, "Harmonics load signature recognition by wavelets transforms," in *Proceedings of International Conference on Electric Utility Deregulation and Restructuring and Power Technologies (DRPT '00)*, pp. 666–671, London, UK, April 2000, IEEE Catalog no. 00EX382.
[4] N. C. F. Tse, "Practical application of wavelet to power quality analysis," in *Proceedings of IEEE Power Engineering Society General Meeting*, p. 5, Montreal, Quebec, Canada, June 2006, IEEE Catalogue no. 06CH37818C, CD ROM.
[5] P. S. Addison, *The Illustrated Wavelet Transform Handbook*, Institute of Physics, Bristol, UK, 2002.
[6] V. L. Pham and K. P. Wong, "Wavelet-transform-based algorithm for harmonic analysis of power system waveforms," *IEE Proceedings: Generation, Transmission and Distribution*, vol. 146, no. 3, pp. 249–254, 1999.
[7] G. Strang and T. Nguyen, *Wavelets and Filter Banks*, Wellesley-Cambridge, Wellesley, Mass, USA, 1996.
[8] S.-J. Huang, C.-T. Hsieh, and C.-L. Huang, "Application of Morlet wavelets to supervise power system disturbances," *IEEE Transactions on Power Delivery*, vol. 14, no. 1, pp. 235–241, 1999.
[9] A. Teolis, *Computational Signal Processing with Wavelets*, Birkhäuser, Boston, Mass, USA, 1998.
[10] M. Misiti, Y. Misiti, and G. Oppenheim, *Wavelet Toolbox for Use with Matlab*, The Mathworks, Natick, Mass, USA, 1996.
[11] S. Mallet, *A Wavelet Tour of Signal Processing*, Academic Press, San Diego, Calif, USA, 1998.
[12] R. A. Carmona, W. L. Hwang, and B. Torrésani, "Multiridge detection and time-frequency reconstruction," *IEEE Transactions on Signal Processing*, vol. 47, no. 2, pp. 480–492, 1999.
[13] R. A. Carmona, W. L. Hwang, and B. Torresani, "Characterization of signals by the ridges of their wavelet transforms," *IEEE Transactions on Signal Processing*, vol. 45, no. 10, pp. 2586–2590, 1997.
[14] A. Antoniadis and G. Oppenheim, Eds., *Wavelets and Statistics*, Lecture Notes in Statistics, Springer, New York, NY, USA, 1995.

Norman C. F. Tse was born in Hong Kong SAR, China, on 7 February, 1961. He graduated from the Hong Kong Polytechnic University (then Hong Kong Polytechnic) in 1985 holding an Associateship in electrical engineering. He obtained M.S. degree from the University of Warwick in 1994. He is a Chartered Engineer, a Corporate Member of the IET, UK (formerly IEE, UK) and the Hong Kong Institution of Engineers. He is now working with the City University of Hong Kong as a Senior Lecturer majoring in building LV electrical power distribution systems. His research interest is in power quality measurement, web-based power quality monitoring, and harmonics mitigation for low-voltage electrical power distribution system in buildings.

L. L. Lai received B.S. (first-class honors) and Ph.D. degrees from Aston University, UK, in 1980 and 1984, respectively. He was awarded D.S. by City University London in 2005 and he is its honorary graduate. Currently he is Head of Energy Systems Group at City University, London. He is also a Visiting Professor at Southeast University, Nanjing, China, and Guest Professor at Fudan University, Shanghai, China. He has authored/coauthored over 200 technical papers. With Wiley, he wrote a book entitled *Intelligent System Applications in Power Engineering - Evolutionary Programming and Neural Networks* and edited one entitled *Power System Restructuring and Deregulation - Trading, Performance and Information Technology.* In 1995, he received a high-quality paper prize from the International Association of Desalination, USA. He was the Conference Chairman of the IEEE/IEE International Conference on Power Utility Deregulation, Restructuring and Power Technologies 2000. He is a Fellow of the IET, an Editor of the IEE Proceedings on Generation, Transmission and Distribution. He was awarded the IEEE Third Millennium Medal, 2000 IEEE Power Engineering Society UKRI Chapter Outstanding Engineer Award, 2003 Outstanding Large Chapter Award, and 2006 Prize Paper Award from Power Generation and Energy Development Committee.